SCIENTIFIC REPORTS

SUBJECT AREAS:
MATERIALS FOR ENERGY AND CATALYSIS
NANOPARTICLES
NANOSCALE MATERIALS
MATERIALS CHEMISTRY

Received
1 November 2012

Accepted
18 February 2013

Published
6 March 2013

Correspondence and requests for materials should be addressed to X.W.L. (xwlou@ntu.edu.sg)

Mesoporous Single-crystal $CoSn(OH)_6$ Hollow Structures with Multilevel Interiors

Zhiyu Wang, Zichen Wang, Haobin Wu & Xiong Wen (David) Lou

School of Chemical and Biomedical Engineering, Nanyang Technological University, 62 Nanyang Drive, Singapore 637459.

Hollow nanostructures represent a unique class of functional nanomaterials with many applications. In this work, a one-pot and unusual "pumpkin-carving" protocol is demonstrated for engineering mesoporous single-crystal hollow structures with multilevel interiors. Single-crystal $CoSn(OH)_6$ nanoboxes with uniform size and porous shell are synthesized by fast growth of $CoSn(OH)_6$ nanocubes and kinetically-controlled etching in alkaline medium. Detailed investigation on reaction course suggests that the formation of a passivation layer of Co(III) species around the liquid-solid interface is critical for the unusual hollowing process. With reasonable understanding on the mechanism involved, this approach shows high versatility for the synthesis of $CoSn(OH)_6$ hollow architectures with a higher order of interior complexity, such as yolk-shell particles and multishelled nanoboxes. The obtained $CoSn(OH)_6$ hollow nanostructures can be easily converted to hollow nanostructures of tin-based ternary metal oxides with excellent photocatalytic and electrochemical properties.

Hollow structures represent a unique class of functional materials characterized by the presence of internal void space[1]. Their characteristic merits include large surface area, potential for high loading capacity, low density, kinetically favorable open structure and so on. The combination of nanoscale interior cavities with chemical functionalities of shell materials endows hollow nanostructures with great technological significance in many areas such as photonic devices, nanoscale reactors, energy storage and delivery vehicles for controlled mass storage/release[1–4]. To meet the application requirements, many templating strategies have been employed for the construction of various hollow particles with narrow size distribution[5–10]. However, the geometry of the products obtained in practice is mostly spherical and the synthesis of non-spherical hollow nanostructures with multiple functionalities, tunable properties and anisotropic texture correlated with multiple axes still suffers from many technological difficulties including less controllable growth of high-curvature shells, the deficiency of non-spherical templates available and poor preservation of the shape with high residual stresses[1]. Recently, several novel approaches have been developed for synthesizing non-spherical nanocages of diverse materials such as noble metals and semiconductors based on different principles including the galvanic replacement, chemical etching, the Kirkendall diffusion effect, quasi-templating process and Ostwald ripening[11–27]. Notwithstanding these advances, the synthesis of non-spherical hollow nanostructures is still in a rudimentary state of development relative to what has been achieved for their spherical counterparts.

In addition to the shape, delicate control over crystalline texture, interior complexity, shell porosity and chemical composition of hollow nanostructures brings additional challenges to their synthesis. To date, the hollow shells obtained are mostly built up by random aggregation of nanoparticles, thus the whole structure appears as polycrystalline or amorphous. Growth of single-crystal hollow structures is intrinsically difficult through the conventional crystal growth from small to big. As for non-spherical hollow nanostructures, single-crystal nanocages have been prepared for only a handful of materials such as noble metals, Cu_2O and Cu_xS_y by different strategies[11–19]. Whereas single-crystal nanoboxes with complex composition and multiple porous shells are not reported so far perhaps due to the significantly increased thermodynamic complexity involved in the synthesis of complex compounds and the difficulty in creating porous single crystals. In this work, we report a facile "pumpkin-carving" strategy for the production of single-crystal $CoSn(OH)_6$ nanoboxes with a uniform size of *ca.* 250 nm and mesoporous shells. The hollowing process of these nanoboxes is in principle different from previous routes towards single-crystal nanocages since it does not involve external surface stabilizing agents, ionic-exchange induced phase transition or Ostwald ripening[11–19]. More remarkably, our synthesis offers additional possibility of engineering single-crystal hollow nanostructures with multilevel interiors. A series of interesting hollow structures, including $CoSn(OH)_6$ yolk-shell particles and multishelled nanoboxes, have been synthesized to demonstrate our concept. For potential applications, the obtained $CoSn(OH)_6$ hollow nanostructures are ideal morphology-controlled templates for generating hollow nanostructures of tin-based ternary metal oxides with excellent photocatalytic and electrochemical properties.

The synthesis of $CoSn(OH)_6$ hollow structures is highly repeatable. As schematically illustrated in Figure 1, perovskite-type $CoSn(OH)_6$ are firstly prepared in an aqueous solution by fast stoichiometric co-precipitation of Sn^{4+}, Co^{2+} and OH^- (equation (1)) in the presence of citrate ions. Its intrinsic cubic crystal structure determines the spontaneous formation of single crystalline nanocubes. Because of the amphoteric nature, $CoSn(OH)_6$ nanocubes can be gradually dissolved in concentrated alkaline solution by coordinating with excess amount of OH^- to form soluble $[Co(OH)_4]^{2-}$ and $[Sn(OH)_6]^{2-}$ at room temperature (equation (2)). In this process, an insoluble boundary layer of Co (III) species can be readily formed on the surface of $CoSn(OH)_6$ crystals due to thermodynamically favorable oxidation of $[Co(OH)_4]^{2-}$ species in air (equation (3)). This passivation layer makes the outer surface of $CoSn(OH)_6$ cubes less reactive than the freshly exposed interiors during the alkaline etching. With continuous evacuation of the core materials across the shell, mesoporous $CoSn(OH)_6$ nanoboxes with well-developed inner cavities are eventually formed without the loss of high crystallinity. By repeated deposition of $CoSn(OH)_6$ layers onto pre-grown $CoSn(OH)_6$ particles (e.g., nanocubes or nanoboxes) and successive alkaline etching, $CoSn(OH)_6$ hollow architectures with complex interiors, including yolk-shell particles and multishelled nanoboxes, can be further produced without the loss of single crystallinity. For the overall process, the major chemical processes involved might be described as follows:

$$Sn^{4+}_{(aq)} + Co^{2+}_{(aq)} + 6OH^{-}_{(aq)} \rightarrow CoSn(OH)_{6(s)} \quad (1)$$

$$CoSn(OH)_{6(s)} + 4OH^{-}_{(aq)} \rightarrow [Co(OH)_4]^{2-}_{(aq)} + [Sn(OH)_6]^{2-}_{(aq)} \quad (2)$$

$$4[Co(OH)_4]^{2-}_{(aq)} + O_{2(g)} \rightarrow 4CoOOH_{(s)} + 2H_2O + 8OH^{-}_{(aq)} \quad (3)$$

Results

Figure 2a–b and Figure S1a (see Supplementary Information) show the field emission scanning electron microscopy (FESEM) images of $CoSn(OH)_6$ products obtained before etching. A panoramic view reveals that the sample consists entirely of uniform nanocubes without impurity particles or aggregates. Transmission electron microscopy (TEM) analysis indicates that these nanocubes are highly uniform with an average edge length of *ca.* 250 nm (Figure 2c–d). The selected area electron diffraction (SAED) pattern of a single nanocube manifests as a regular array of diffraction spots along the <001> zone axis of $CoSn(OH)_6$ crystal (Figure 2f). The [010] and [100] directions are parallel to adjacent sides of the nanocubes (Figure 2e), indicating that the nanocubes are single-crystalline and enclosed by six nominal {100} facets. The X-ray powder diffraction (XRD) analysis also confirms the high crystallinity of these nanocubes, as characterized by sharp diffraction peaks from perovskite-type $CoSn(OH)_6$ (JCPDS card no. 13–356, space group: *Pn3m*, $a_0 = 7.75$ Å) (Figure 3a). No signals from possible impurities such as $Co(OH)_2$ or SnO_2 are detected as a result of the stoichiometrically controlled co-precipitation of Co^{2+} and Sn^{4+} in the presence of excess amount of OH^-. N_2 adsorption/desorption measurement shows that these nanocubes possess a Brunauer-Emmett-Teller (BET) specific surface area of 80 $m^2 g^{-1}$ (see Supplementary Figure S2b).

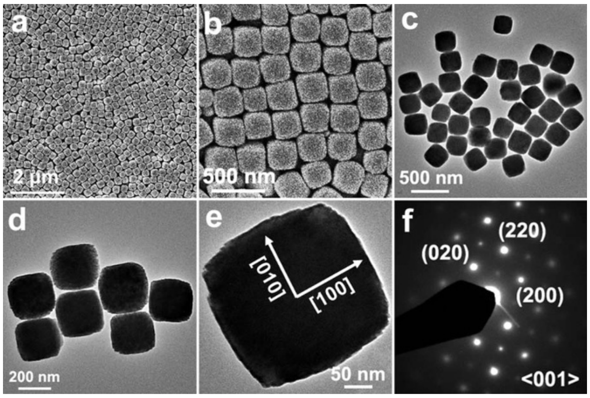

Figure 2 | Morphology characterization. (a, b) FESEM images and (c, d) TEM images of $CoSn(OH)_6$ nanocubes. (e) a free-standing nanocube enclosed by six nominal {100} facets, and its corresponding SAED pattern (f) showing the perfect single-crystalline feature.

In a highly alkaline medium, $CoSn(OH)_6$ can be gradually dissolved at ambient conditions by forming soluble complexes with OH^- in excess (equation (2)). This simple chemistry enables us to create single-crystalline hollow structures through controlled etching of surface-stabilized $CoSn(OH)_6$ nanocubes. The XRD analysis (Figure 3a) and FESEM examination (Figure 4a) indicate that the

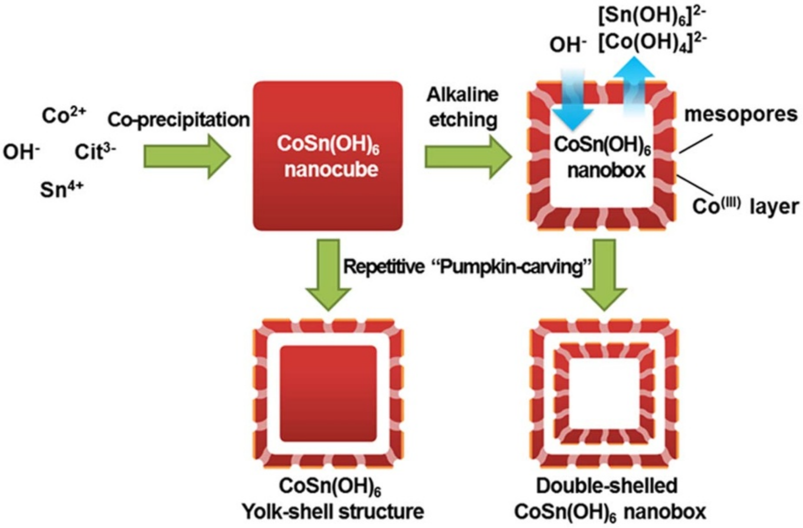

Figure 1 | Formation mechanism of $CoSn(OH)_6$ hollow nanostructures. Schematic illustration for the formation of single-crystal $CoSn(OH)_6$ yolk-shell particles and multishelled nanoboxes (citrate anion is denoted as Cit^{3-}).

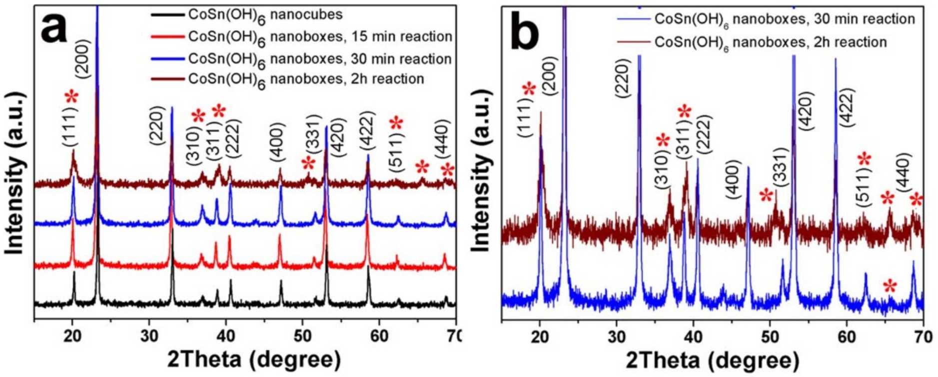

Figure 3 | **Phase analysis.** (a) XRD profiles of $CoSn(OH)_6$ nanocubes and nanoboxes obtained after the reaction of 15 min–2 h; (b) Enlarged XRD pattern of $CoSn(OH)_6$ sample obtained after 30 min and 2 h reaction, in which the signals of CoO(OH) phase are marked with red asterisks.

as-obtained nanoboxes well inherit the composition and uniform dimensions of precursor $CoSn(OH)_6$ nanocubes with an edge length of *ca.* 250 nm. Their interior space can be directly examined by FESEM for cracked nanoboxes, as shown in Figure 4b. The hollow interior and geometrical structure of as-obtained nanoboxes are further elucidated by TEM, as shown in Figure 4c–e and Supplementary Figure S1b. In agreement with the FESEM findings, high uniformity of the nanoboxes is revealed while the inner cavities are clearly revealed by the sharp contrast between the shells and hollow interiors. The shell of these nanoboxes is uniform with a thickness of around 30–40 nm and numerous mesopores (Figure 4f and Figure S3). Despite the fast etching, the crystalline texture of the nanoboxes is still well preserved. Remarkably, the SAED analysis along the <001> zone axis indicates that these nanoboxes are also single crystals bounded with {100} facets (Figure 4h). In the high-resolution TEM (HRTEM) image, mutually perpendicular lattice fringes with the same interspacing of 0.38 nm can be clearly seen, corresponding to the (200) and (020) planes of $CoSn(OH)_6$ crystal (Figure 4i). The elemental mapping measurement of a single nanobox confirms the co-existence and homogenous dispersion of Sn, Co and O elements within the nanobox (Figure 4j). The nitrogen adsorption/desorption isotherm of these nanoboxes shows a typical type IV curve with a type H4 hysteresis loop, as shown in Figure S2a. The capillary condensation occurs at a relative pressure higher than 0.9, indicating the presence of mesopores which gives rise to a high BET specific surface area of 104 $m^2 g^{-1}$. The wide hysteresis loop together with the pore size distributions from both branches of the isotherm reveals the presence of irregular pores with entrance size centered around 3–6 nm[28]. Such pores are produced by alkaline etching on the surface defects or high-curvature edges of the single-crystalline nanocubes, and which then serve as the mass diffusion pathway for the evacuation of the interior material of $CoSn(OH)_6$ crystals.

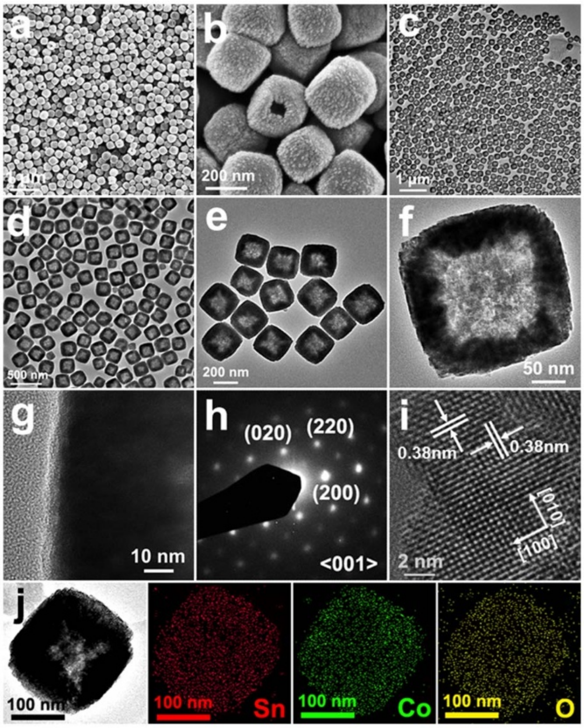

Figure 4 | **Morphology and composition characterization.** (a, b) FESEM images and (c–e) TEM images of $CoSn(OH)_6$ nanoboxes; (f) a nanobox with well-developed interior; (g) a TEM image showing the shell structure of a nanobox, on which a very thin layer of Co (III) species is covered on the outer surface; (h) SAED pattern of a single nanobox; (i) HRTEM image along a zone axis of <001>; (j) elemental mapping showing the homogenous dispersion of Sn, Co and O element in $CoSn(OH)_6$ nanoboxes.

A time-course investigation of the reaction reveals that the formation of $CoSn(OH)_6$ nanoboxes can be separated into two distinct stages. Firstly, solid $CoSn(OH)_6$ nanocubes are formed within one hour as a result of the fast precipitation reaction and the inherent growth habit of cubic crystals (Figure 2). In this process, sodium citrate is found critical for the formation of discrete and uniform nanocubes under the non-equilibrium conditions of high feedstock concentrations because of its well-known capability of homogenizing crystal growth[29,30]. In the absence of sodium citrate, poorly dispersed nanocubes are produced with many impurity particles because of uncontrolled nucleation and rapid crystal growth (Figure 5a–b). After excess amount of NaOH solution is added into the reaction medium, small voids emerge inside the nanocubes within a short period of one minute due to fast dissolution of $CoSn(OH)_6$ crystals in highly alkaline medium, as shown in Figure 5c. With continuous etching for 10 min, the voids become larger as a result of the unceasing outflow of soluble ions (Figure 5d) and eventually evolve to well-developed interiors after reaction for 15 min (Figure 4). Notably, during the process the exterior shape, size and chemical composition of the $CoSn(OH)_6$ particles are almost identical. Even reacting for a longer time of 30 min–2 h, the overall structure still remains largely unaltered despite the severe growth of impurity particles on the surface (Figure 5e–f). Evidently, the outer surface of these nanoboxes has been adequately protected from the violent attack of OH^- anions although the system does not involve any common stabilizing agents such as polyvinylpyrrolidone (PVP) and sodium dodecyl sulfate (SDS), and phase transition induced by ionic exchange[11,12,14–16]. Normally, this is hardly achieved at ambient conditions especially

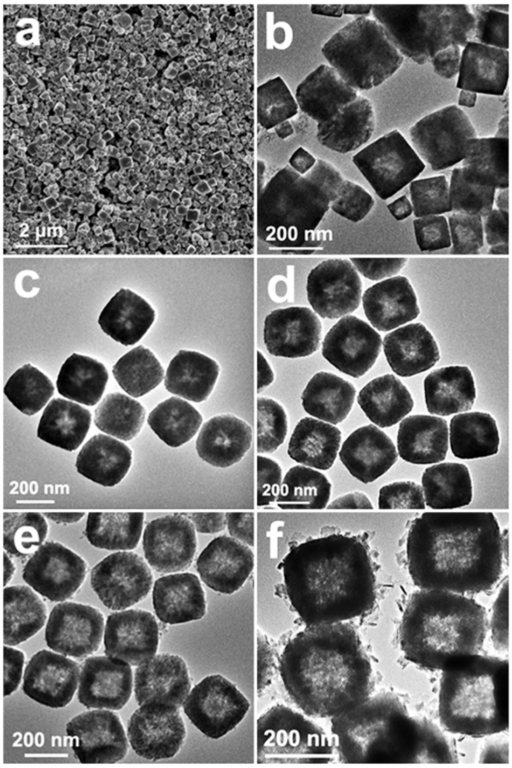

Figure 5 | Morphology characterization. FESEM and TEM images of $CoSn(OH)_6$ products obtained in the absence of sodium citrate (a, b). (c–f) $CoSn(OH)_6$ products obtained at different reaction times of 1 min (c); 10 min (d); 30 min (e) and 2 h (f).

when the shell and the precursor materials have the same composition, high crystallinity and relatively similar reactivity.

Discussion

To uncover the mechanism involved in the unusual hollowing process of $CoSn(OH)_6$ nanocubes, TEM is employed to examine their surface characteristics. Interestingly, a very thin layer of distinct material is observed on the outer surface of the nanoboxes (Figure 4g and Supplementary Figure S3). To get more clues on its composition, the products obtained for longer reaction durations (e.g., 30 min–2 h, Figure 5f) are examined by XRD analysis because the mass fraction of this layer is too small to be detected in the samples obtained with a short reaction time. Weak signals from the CoO(OH) phase (JCPDS card no. 26–480) are detected along with the pronounced peaks of $CoSn(OH)_6$, as shown in Figure 3b. Clearly, the gradual oxidation of $[Co(OH)_4]^{2-}$ has occurred by reacting with the oxygen dissolved in solution even at room temperature. This oxidation reaction is thermodynamically favorable and can even be accelerated in a concentrated alkaline medium because of the significantly reduced redox potential[31,32]. As a result, a layer of insoluble Co(III) species may be deposited onto the surface of $CoSn(OH)_6$ nanocubes. This stable layer serves as a physical barrier against the alkaline etching such that the dissolution of the nanocubes is restricted to occur on the less covered surface or high-curvature edges where the reactivity is higher. The unceasing inward diffusion of OH^- anions and outward flow of soluble metal complexes eventually lead to the formation of well-developed interiors inside the stabilized nanocubes through continuous evacuation of the core material across the porous shell. To verify the critical role of Co(III) species played in the formation of $CoSn(OH)_6$ nanoboxes, the reaction is conducted under the protection of inert gas (Ar) to suppress the oxidation of $[Co(OH)_4]^{2-}$ complex while keeping other conditions unchanged. Interestingly, the etching of $CoSn(OH)_6$ nanocubes indeed preferentially takes place from the outer surface of the crystal to produce rough solid nanospheres instead of hollow structures (see Supplementary Figure S4). Apparently, the presence of Co(III) species can effectively passivate the outer surface of $CoSn(OH)_6$ nanocubes, and is therefore essential to maintain the shell structure of the nanoboxes upon alkaline etching. Moreover, the effect of sodium citrate on the formation of $CoSn(OH)_6$ nanoboxes is also investigated. Regardless of its presence or not at any stage of the reaction, hollow structures can always be obtained by the same route (see experimental details, Figure 5a–b and Supplementary Figure S5). Clearly, sodium citrate is not crucial to the hollowing process of the nanocubes in the present system, although this class of organic salts (e.g., sodium tartrate) is sometimes involved for the construction of hollow shells of metal oxides[17].

With a good understanding of the hollowing process, the "pumpkin-carving" strategy can be further extended for the synthesis of $CoSn(OH)_6$ hollow architectures with a higher order of interior complexity. The synthesis protocol for making these unique structures is designed based on the repeated deposition of $CoSn(OH)_6$ layers onto pre-grown seed particles such as nanocubes and nanoboxes and subsequent alkaline etching. In this process, the dissolution of $CoSn(OH)_6$ crystals mainly occurs between the passivated outer surface of seed particles and newly deposited crystal layers. As a result of localized "pumpkin-carving" process, well-defined intershell cavities are generated within $CoSn(OH)_6$ crystals, leading to the formation of yolk-shell particles or double-shelled nanoboxes (Figure 6a–g). For both structures, the cubic shape of the seed particles is well preserved and the thickness of newly generated shells is around 10–20 nm. The formation of core-shell structure endows them with higher BET surface areas (yolk-shell particles: 111 $m^2\ g^{-1}$; double-shelled nanoboxes: 120 $m^2\ g^{-1}$) than that of $CoSn(OH)_6$ nanoboxes (see Supplementary Figure S2c–d). The crystal phase is not altered in these hollow architectures as shown by XRD analysis (see Supplementary Figure S6). Unexpectedly, these hollow architectures can still remain single crystalline despite the repetitive crystal deposition and chemical etching, as suggested by SAED analysis (Figure 6e) and HRTEM examination (see Supplementary Figure S7). This is hardly achieved by the conventional approaches of templating casting or Ostwald ripening[26,33–37]. Depending on the etching conditions, the intershell spacing of double-shelled nanoboxes can be readily tailored in a range of 5–30 nm to generate hollow structures with tunable eccentricity (Figure 6f–g). Encouragingly, $CoSn(OH)_6$ nanoboxes with multiple shells (up to 4 shells) can be also fabricated by repeating the localized "pumpkin-carving" process, as shown in Figure 6h–i. Such structures would enable the better control over local microenvironment for chemical mixing and mass transport. As a result, novel physicochemical properties are anticipated.

For potential applications, $CoSn(OH)_6$ nanoboxes are ideal morphology-controlled precursor for making hollow nanostructures of tin-based complex metal oxides. For example, polycrystalline Co-Sn-O nanoboxes can be obtained by thermal annealing of $CoSn(OH)_6$ boxes at a high temperature of 700°C in N_2 flow (equation (4)). Despite of decreased crystallinity, the conversation from $CoSn(OH)_6$ to Co-Sn-O nanoboxes undergoes a topotactic transformation process without structural collapse (see Supplementary Figure S6). Detailed XRD analysis reveals that the Co-Sn-O nanoboxes are actually a composite of polycrystalline Co_2SnO_4 and SnO_2 (see Supplementary Figure S8a and Supplementary Figure S8c). Owing to the unique composition and structure, they can be employed as one photocatalyst for the degradation of organic pollutants under the illumination of light. In this structure, the coupled system of semiconductors may slow down the recombination of photogenerated electrons and holes due to more efficient separation of electrons and holes, making the oxidation of organic species much easier[38–40]. The large surface area of hollow structure may introduce

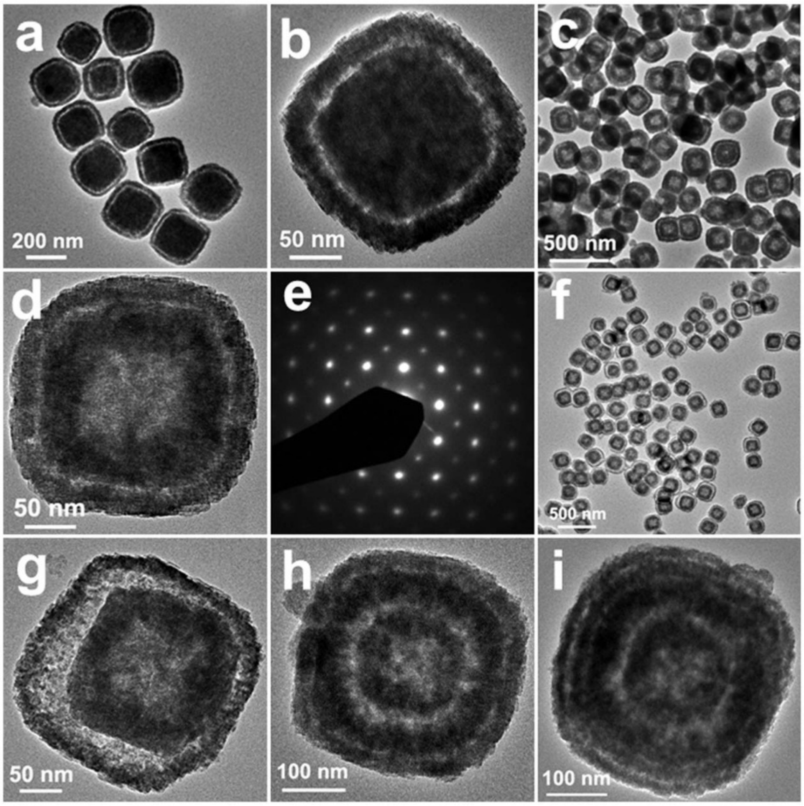

Figure 6 | **Morphology characterization.** TEM images of $CoSn(OH)_6$ hollow architectures with multilevel interiors: (a, b) yolk-shell particles; (c, d) double-shelled nanoboxes; (e) SAED pattern of a double-shelled nanobox; (f, g) double-shelled nanoboxes with larger intershell cavities; (h) a triple-shelled nanobox; (i) a quadruple-shelled nanobox.

more reactive sites on the surface of the photocatalyst, while increasing the adsorption ability of organic molecules. Their nanosized thin shell also allows fast diffusion of photogenerated electron-hole pairs onto the surface of the photocatalyst. Due to significantly enhanced kinetics, high photocatalytic efficiency is thus highly anticipated for these Co-Sn-O nanoboxes. To evidence their photocatalytic activities, the photocatalytic decomposition of methylene blue (MB) is performed as a probe reaction under the irradiation of UV light. Figure 7a shows the evolution of MB adsorption spectra in the presence of polycrystalline Co-Sn-O nanoboxes, in which the characteristic adsorption peak of MB ($\lambda = 663$ nm) diminishes gradually as the illumination time increases. After the UV irradiation for 210 min, Co-Sn-O nanoboxes are able to degrade over 95% of the original organic dye, as shown in Figure 7b. In the absence of UV irradiation with the photocatalyst or in the presence of irradiation without the photocatalyst, however, the MB is hardly decomposed while other conditions remain identical, which further confirm the photocatalytic activity of Co-Sn-O nanoboxes. For $CoSn(OH)_6$ nanoboxes, low photocatalytic ability towards the MB is observed perhaps due to poor semiconductivity, although some perovskite-type metal hydroxystannates (e.g., $CaSn(OH)_6$ and $ZnSn(OH)_6$) can be photocatalytically active for the degradation of organic compounds[27,41]. These results indicate that the polycrystalline Co-Sn-O nanoboxes have a very appealing prospect on the purification of the waste water polluted by organic dyes.

$$2CoSn(OH)_{6(s)} \xrightarrow{\Delta} Co_2SnO_{4(s)} + SnO_{2(s)} + 6H_2O_{(g)}\ (T = 700^{o}C) \tag{4}$$

$$CoSn(OH)_{6(s)} \xrightarrow{\Delta} CoSnO_{3(s)} + 3H_2O_{(g)}\ (T = 500^{o}C) \tag{5}$$

Another interesting application of tin-based metal oxide nanoboxes is found in lithium-ion batteries (LIBs) because of their high capacity (generally around 500–600 mA h g^{-1}) for lithium storage. For this purpose, amorphous $CoSnO_3$ nanoboxes are produced by thermal stoichiometric dehydration of $CoSn(OH)_6$ boxes at a lower temperature of 500°C (equation (5)), as shown in Supplementary Figure S8b and Supplementary Figure S8c. Within $CoSnO_3$ nanoboxes, all the elements are homogenously dispersed to form an atomically mixed buffering matrix, which effectively mitigates the electrode destruction and enhances the ionic mobility[42]. By sharing the substantial advantages of hollow nanostructures such as shorten diffusion pathway, large surface area and reduced internal stress by free interior cavities, $CoSnO_3$ nanoboxes exhibit greatly improved performance when evaluated as an anode material in LIBs. They can deliver high initial capacity of over 1600 mA h g^{-1} within a cut-off window of 0.01–1.5 V at a current density of 200 mA g^{-1} (Figure 7c). From the second cycle onwards, $CoSnO_3$ nanoboxes exhibit high capacities of 520–620 mA h g^{-1} with stable capacity retention of over 80–90% for 60 cycles (Figure 7d). This value is much higher than the theoretical capacity of commercial carbonaceous electrodes (372 mA h g^{-1}) and is superior to many ternary metal oxide electrodes such as $CaSnO_3$, $CoSnO_3$, Zn_2SnO_4 and $ZnCo_2O_4$[43–45]. With surface coating of a thin carbon layer, the calendar life of $CoSnO_3$ nanoboxes can be significantly prolonged to over 400 cycles with acceptable capacities of over 450 mA h g^{-1}[42]. Evidently, the combination of hollow structures with unique composition of $CoSnO_3$ has shown great advantages for high-performance lithium storage.

In summary, we have demonstrated an unusual "pumpkin-carving" route for the formation of mesoporous single-crystal $CoSn(OH)_6$ nanoboxes. The process involves two distinct stages, the fast formation of $CoSn(OH)_6$ nanocubes, and surface-protected etching in an alkaline medium. The formation of a Co(III) passivating layer is found critical for this unusual hollowing process. The as-obtained nanoboxes are highly uniform with a size of *ca.* 250 nm.

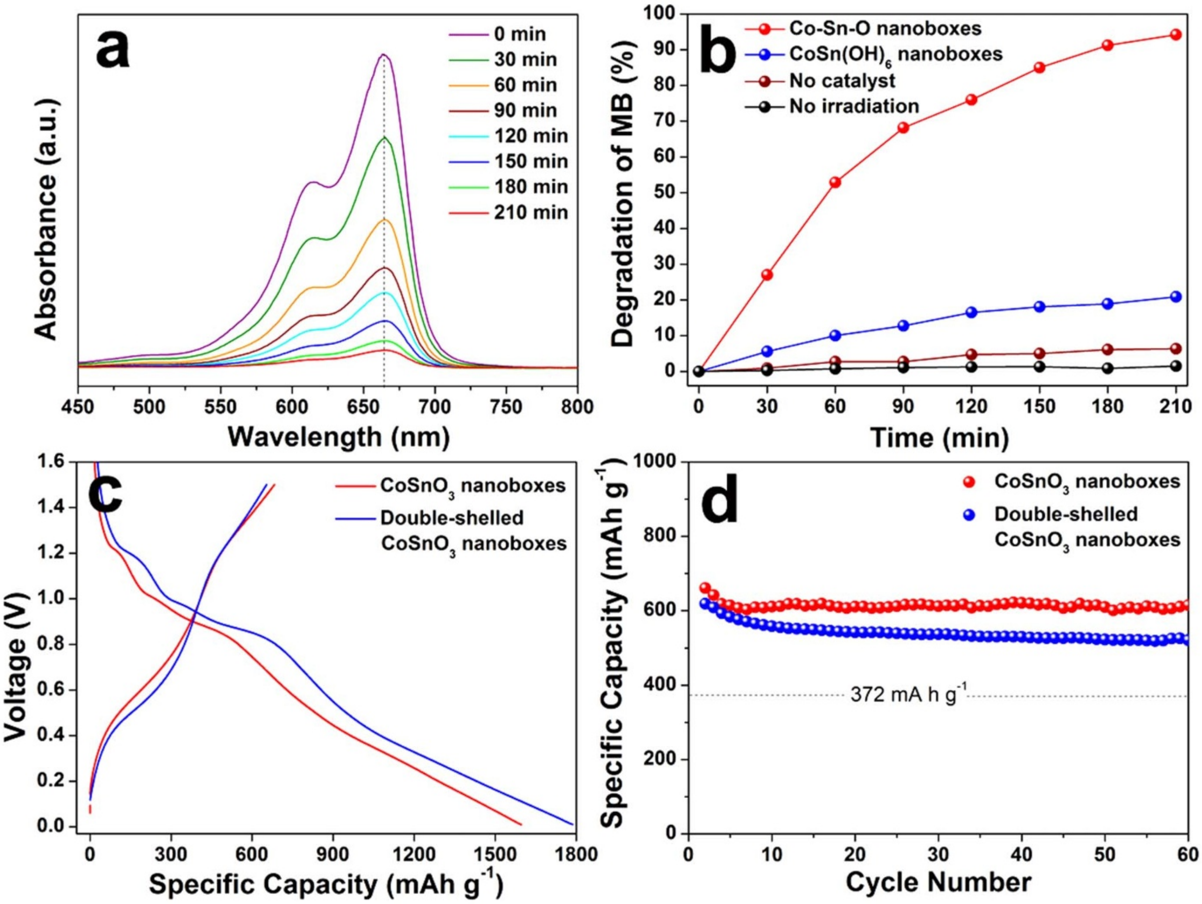

Figure 7 | Photocatalytic and electrochemical properties. (a) Absorption spectra of solutions of MB at different time intervals since the photocatalytic reaction started under continuous illumination of UV light (λ = 254 nm) in the presence of Co-Sn-O nanoboxes; (b) photocatalytic performance of Co-Sn-O and $CoSn(OH)_6$ nanoboxes for the degradation of MB under UV light; (c) discharge/charge voltage curves and (d) cycling performance of $CoSnO_3$ nanoboxes with single and double shells at a current density of 200 mA g^{-1} between 0.01–1.5 V.

Despite being single-crystal, the shell wall is highly mesoporous with a thickness of 30–40 nm and a large surface area of 104 $m^2\,g^{-1}$. This approach can be readily extended for the synthesis of $CoSn(OH)_6$ hollow architectures with a higher order of interior complexity, such as yolk-shell particles and multishelled nanoboxes, which further evidences the versatility of this strategy. It is remarkable that multi-shelled nanoboxes can remain as single-crystalline. To demonstrate potential applications, tin-based metal oxide hollow nanostructures with tunable composition and crystalline texture are further synthesized by thermal annealing of $CoSn(OH)_6$ nanoboxes at different temperatures, which exhibit excellent photocatalytic and electrochemical properties. We believe the concepts demonstrated in this work might shed some light on the fabrication and application of single-crystal hollow structures with engineered interior and porous shells.

Methods

Synthesis of $CoSn(OH)_6$ nanocubes. All the reagents are of analytical grade and used without further purification. In a typical synthesis, 5 mL of ethanol solution of $SnCl_4$ (1 mmol) was added into 35 mL of a mixture aqueous solution containing $CoCl_2$ (1 mmol) and sodium citrate (1 mmol) under stirring, followed by dropwise addition of 5 mL of aqueous solution of NaOH (2 M) at room temperature. After 1 h, the resulting pink product was harvested by several rinse-centrifugation cycles with deionized (DI) water and ethanol for further characterization.

Synthesis of single-shelled $CoSn(OH)_6$ nanoboxes. All the reagents are of analytical grade and used without further purification. $CoSn(OH)_6$ nanoboxes can be obtained by two routes: (i) 20 mL of aqueous solution of NaOH (8 M) was successively added into the suspension containing $CoSn(OH)_6$ nanocubes without rinsing and the reaction was lasted for 15 min at room temperature; (ii) 20 mL of aqueous solution of NaOH (8 M) was added into the suspension of $CoSn(OH)_6$ nanocubes in 40 mL of DI water . After reaction at room temperature for 15 min, the resulting pink product was harvested by several rinse-centrifugation cycles with DI water and ethanol for further characterization.

Synthesis of multishelled $CoSn(OH)_6$ nanoboxes and yolk-shell structure. All the reagents are of analytical grade and used without further purification. For the synthesis of double-shelled $CoSn(OH)_6$ nanoboxes, 5 mL of ethanol solution of $SnCl_4$ (1 mmol) was added into 35 mL of a mixture suspension containing as-obtained single-shelled $CoSn(OH)_6$ nanoboxes, $CoCl_2$ (1 mmol) and sodium citrate (1 mmol) under stirring, followed by dropwise addition of 5 mL of aqueous solution of NaOH (2 M) at room temperature. After reaction for 1 h, 20 mL of aqueous solution of NaOH (8 M) was added into the suspension and the reaction was lasted for 15 min to obtain the final products. $CoSn(OH)_6$ nanoboxes with triple and quadruple shells were synthesized by a similar procedure with double-shelled and triple-shelled nanoboxes as the seed materials, respectively. $CoSn(OH)_6$ yolk-shell particles were also made by a similar method but with $CoSn(OH)_6$ nanocubes as the seed material. All the samples were harvested by several rinse-centrifugation cycles with DI water and ethanol for further characterization.

Synthesis of $CoSn(OH)_6$ nanospheres. All the reagents are of analytical grade and used without further purification. The synthesis of $CoSn(OH)_6$ nanospheres was conducted under inert conditions at room temperature. In a typical synthesis, 5 mL of ethanol solution of $SnCl_4$ (1 mmol) was added into 35 mL of a mixture solution containing $CoCl_2$ (1 mmol) and sodium citrate (1 mmol) under stirring in Ar flow, followed by dropwise addition of 5 mL of aqueous solution of NaOH (2 M). After 1 h, 20 mL of aqueous solution of NaOH (8 M) was injected into the precursor solution with stirring for 15 min. The resulting pink products were harvested by several rinse-centrifugation cycles with DI water and ethanol for further characterization.

Material characterization. The morphology and crystalline structure of as-obtained samples were characterized with field-emission scanning electron microscopy (FESEM, JEOL, JSM-6700F) and transmission electron microscopy (TEM, JEOL, JEM-2010 and JEM-2100F, operated at 200 kV). Powder X-ray diffraction (XRD) patterns were recorded on a Bruker D8-Advance X-ray diffractometer with Cu Ka radiation ($\lambda = 1.5406$ Å). The surface area properties of the samples were measured by Micrometrics ASAP 2020 Surface Area and Porosity Analyzer.

Photocatalytic degradation of methylene blue (MB). For photocatalytic degradation of MB, polycrystalline Co-Sn-O nanoboxes were first synthesized by annealing CoSn(OH)$_6$ nanoboxes in N_2 flow at 700°C for 2 h with a slow ramp rate of 1°C min^{-1}. Then 50 mg of Co-Sn-O nanoboxes was dispersed in 50 mL of aqueous solution of MB (5 mg L^{-1}). Prior to irradiation, the mixture solution was stirred in dark for 30 min to reach the adsorption/desorption equilibrium. After the solution was irradiated by UV light ($\lambda = 254$ nm) for given durations under stirring, solid photocatalysts were removed by high-speed centrifugation and UV-vis absorption spectrum of the as-obtained solutions was measured on a Cary 50 UV-vis spectrophotometer with DI water as the reference. The concentration of MB was determined from the absorbance at the wavelength of 663 nm using a UV-visible spectrophotometer. The degradation efficiency (%D) was calculated from the following formula: $\%D = 100 \times [(C_0 - C_t)/C_0] = 100 \times [(A_0 - A_t)/A_0]$ (C_0 = the initial concentration of MB; C_t = the concentration of MB at time t; A_0 = the initial absorbance of MB; A_t = the absorbance of MB at time t).

Electrochemical measurements. For electrochemical measurement, amorphous $CoSnO_3$ nanoboxes were first prepared by successively annealing in N_2 flow at 150°C, 300°C and 500°C with a slow ramp rate of 1°C min^{-1}. At each stage, the temperature was maintained for 2 h. The electrochemical measurements were conducted using two-electrode Swagelok cells with pure lithium foil as the counter and reference electrode at room temperature. The working electrode consists of active materials ($CoSnO_3$ nanoboxes with single or double shells), carbon black (Super-P-Li) and polyvinylidene difluoride (PVDF) in a weight ratio of 7 : 2 : 1. The electrolyte used is 1.0 M $LiPF_6$ in a 50 : 50 (w/w) mixture of ethylene carbonate and diethyl carbonate. The galvanostatic charge/discharge tests were performed using a Neware battery tester at a current density of 200 mA g^{-1} within a cut-off voltage window of 0.01–1.5 V.

1. Lou, X. W., Archer, L. A. & Yang, Z. C. Hollow micro-/nanostructures: synthesis and applications. *Adv. Mater.* **20**, 3987–4019 (2008).
2. Yang, H. G. & Zeng, H. C. Preparation of hollow anatase TiO_2 nanospheres via Ostwald ripening. *J. Phys. Chem. B* **108**, 3492–3495 (2004).
3. Lai, X. Y., Halpert, J. E. & Wang, D. Recent advances in micro-/nano-structured hollow spheres for energy applications: from simple to complex systems. *Energy Environ. Sci.* 5604–5618 (2011).
4. Hu, J., Chen, M., Fang, X. S. & Wu, L. M. Fabrication and application of inorganic hollow spheres. *Chem. Soc. Rev.* **40**, 5472–5491 (2011).
5. Zhong, Z. Y., Yin, Y. D., Gates, B. & Xia, Y. N. Preparation of mesoscale hollow spheres of TiO_2 and SnO_2 by templating against crystalline arrays of polystyrene beads. *Adv. Mater.* **12**, 206–209 (2000).
6. Kim, S. W., Kim, M., Lee, W. Y. & Hyeon, T. Fabrication of hollow palladium spheres and their successful application to the recyclable heterogeneous catalyst for Suzuki coupling reactions. *J. Am. Chem. Soc.* **124**, 7642–7643 (2002).
7. Caruso, F., Caruso, R. A. & Mohwald, H. Nanoengineering of inorganic and hybrid hollow spheres by colloidal templating. *Science* **282**, 1111–1114 (1998).
8. Zoldesi, C. I. & Imhof, A. Synthesis of monodisperse colloidal spheres, capsules, and microballoons by emulsion templating. *Adv. Mater.* **17**, 924–928 (2005).
9. Peng, Q., Dong, Y. J. & Li, Y. D. ZnSe semiconductor hollow microspheres. *Angew. Chem. Int. Ed.* **42**, 3027–3030 (2003).
10. Zhang, L. *et al.* Magnetic hollow spheres of periodic mesoporous organosilica and Fe_3O_4 nanocrystals: fabrication and structure control. *Adv. Mater.* **20**, 805–809 (2008).
11. Kuo, C. H. & Huang, M. H. Fabrication of truncated rhombic dodecahedral Cu_2O nanocages and nanoframes by particle aggregation and acidic etching. *J. Am. Chem. Soc.* **130**, 12815–12820 (2008).
12. Xiong, Y. J. *et al.* Corrosion-based synthesis of single-crystal Pd nanoboxes and nanocages and their surface plasmon properties. *Angew. Chem. Int. Ed.* **44**, 7913–7917 (2005).
13. Sun, Y. G. & Xia, Y. N. Shape-controlled synthesis of gold and silver nanoparticles. *Science* **298**, 2176–2179 (2002).
14. Sui, Y. M. *et al.* Synthesis of Cu_2O nanoframes and nanocages by delective oxidative etching at room temperature. *Angew. Chem. Int. Ed.* **49**, 4282–4285 (2010).
15. Cao, H. L. *et al.* High symmetric 18-facet polyhedron nanocrystals of Cu_7S_4 with a hollow nanocage. *J. Am. Chem. Soc.* **127**, 16024–16025 (2005).
16. Jiao, S. H., Xu, L. F., Jiang, K. & Xu, D. S. Well-defined non-spherical copper sulfide mesocages with single-crystalline shells by shape-controlled Cu_2O crystal templating. *Adv. Mater.* **18**, 1174–1177 (2006).
17. Lu, C. H. *et al.* One-pot synthesis of octahedral Cu_2O nanocages via a catalytic solution route. *Adv. Mater.* **17**, 2562–2567 (2005).
18. Yang, X. F. *et al.* Formation mechanism of $CaTiO_3$ hollow crystals with different microstructures. *J. Am. Chem. Soc.* **32**, 14279–14287 (2010).
19. Wang, W. Z., Poudel, B., wang, D. Z. & Ren, Z. F. Synthesis of PbTe nanoboxes using a solvothermal technique. *Adv. Mater.* **17**, 2110–2114 (2005).
20. Yin, Y. D. *et al.* Formation of hollow nanocrystals through the nanoscale kirkendall effect. *Science* **304**, 711–714 (2004).
21. Fan, H. J., Gösele, U. & Zacharias, M. Formation of nanotubes and hollow nanoparticles based on kirkendall and diffusion processes: a review. *Small* **3**, 1660–1671 (2007).
22. Sun, Y. G., Mayers, B. T. & Xia, Y. N. Template-engaged replacement reaction: a one-step approach to the large-scale synthesis of metal nanostructures with hollow interiors. *Nano Lett.* **2**, 481–485 (2002).
23. An, K. *et al.* Synthesis of uniform hollow oxide nanoparticles through nanoscale acid etching. *Nano Lett.* **8**, 4252–4258 (2008).
24. He, T., Chen, D. R., Jiao, X. L. & Wang, Y. L. Co_3O_4 nanoboxes: Surfactant-templated fabrication and microstructure characterization. *Adv. Mater.* **18**, 1078–1082 (2006).
25. Lou, X. W., Yuan, C., Zhang, Q. & Archer, L. A. Platinum-functionalized octahedral silica nanocages: synthesis and characterization. *Angew. Chem. Int. Ed.* **45**, 3825–3829 (2006).
26. Wang, Z. Y. *et al.* Engineering nonspherical hollow structures with complex interiors by template-engaged redox etching. *J. Am. Chem. Soc.* **132**, 16271–16277 (2010).
27. Wang, L. L. *et al.* Single-crystalline $ZnSn(OH)_6$ hollow cubes via self-templated synthesis at room temperature and their photocatalytic properties. *J. Mater. Chem.* **21**, 4352 (2011).
28. Kruk, M. & Jaroniec, M. Gas adsorption characterization of ordered organic-inorganic nanocomposite materials. *Chem. Mater.* **13**, 3169–3183 (2001).
29. Enustun, B. V. & Turkevich, J. Coagulation of colloidal gold. *J. Am. Chem. Soc.* **85**, 3317–3328 (1963).
30. Turkevic, J. & Kim, G. Palladium: preparation and catalytic properties of particles of uniform size. *Science* **169**, 873–879 (1970).
31. Chambers, C. & Holliday, A. K. *Modern inorganic chemistry.* 404 (Butterworth & Co. Ltd., 1975).
32. Earnshaw, A. & Greenwood, N. N. *Chemistry of the Elements (2nd Ed).* 1123 (Butterworth-Heinneman Press, 1997).
33. Zhang, L. & Wang, H. Interior structural tailoring of Cu_2O shell-in-shell nanostructures through multistep ostwald ripening. *J. Phys. Chem. C* **115**, 18479 (2011).
34. Lou, X. W., Yuan, C. L. & Archer, L. A. Shell-by-shell synthesis of tin oxide hollow colloids with nanoarchitectured walls: cavity size tuning and functionalization. *Small* **3**, 261–265 (2007).
35. Lou, X. W., Yuan, C. L. & Archer, L. A. Double-walled SnO_2 nano-cocoons with movable magnetic cores. *Adv. Mater.* **19**, 3328–3332 (2007).
36. Yang, M., Ma, J., Zhang, C. L., Yang, Z. Z. & Lu, Y. F. General synthetic route toward functional hollow spheres with double-shelled structures. *Angew. Chem. Int. Ed.* **44**, 6727–6730 (2005).
37. Yec, C. C. & Zeng, H. C. Synthetic architecture of multiple core-shell and yolk-shell structures of $(Cu_2O@)nCu_2O$ ($n = 1$–4) with centricity and eccentricity. *Chem. Mater.* **24**, 1917–1929 (2012).
38. Uddin, M. T. *et al.* Nanostructured SnO_2-ZnO heterojunction photocatalysts showing enhanced photocatalytic activity for the degradation of organic dyes. *Inorg. Chem.* **51**, 7764–7773 (2012).
39. Kang, J., Qin, K., Xie, Z. X. & Zheng, L. S. Fabrication of the SnO_2/a-Fe_2O_3 hierarchical heterostructure and its enhanced photocatalytic property. *J. phys. Chem. C* **115**, 7874–7879 (2011).
40. Niu, M. T. *et al.* Hydrothermal synthesis, structural characteristics, and enhanced photocatalysis of SnO_2/a-Fe_2O_3 semiconductor nanoheterostructures. *Acs Nano* **4**, 681–688 (2010).
41. Meng, S. *et al.* Sonochemical synthesis, characterization and photocatalytic properties of a novel cube-shaped $CaSn(OH)_6$. *Catal. Commun.* **12**, 972–975 (2011).
42. Wang, Z. Y., Wang, Z. C., Liu, W. T., Xiao, W. & Lou, X. W. Amorphous $CoSnO_3$@C nanoboxes with superior lithium storage capability. *Energy Environ. Sci.* **6**, 87–91 (2013).
43. Rong, A. *et al.* Hydrothermal Synthesis of Zn_2SnO_4 as Anode Materials for Li-Ion Battery. *J. Phys. Chem. B* **110**, 14754–14760 (2006).
44. Sharma, N., Shaju, K. M., Subba Rao, G. V. & Chowdari, B. V. R. Sol–gel derived nano-crystalline $CaSnO_3$ as high capacity anode material for Li-ion batteries. *Electrochem. Commun.* **4**, 947–952 (2002).
45. Connor, P. A. & Irvine, J. T. S. Novel tin oxide spinel-based anodes for Li-ion batteries. *J. Power Source.* **97–98**, 223–225 (2001).

Author contributions

Z.Y. Wang and X.W. Lou designed the experiment. Z.Y. Wang and Z.C. Wang carried out the experiment. H.B. Wu helped in synthesis, TEM characterization and data analysis. Z.Y. Wang and X.W. Lou analyzed the data and wrote the manuscript.

Additional information

Supplementary information accompanies this paper at http://www.nature.com/scientificreports

Competing financial interests: The authors declare no competing financial interests.

How to cite this article: Wang, Z.Y., Wang, Z.C., Wu, H.B. & Lou, X.W.D. Mesoporous Single-crystal $CoSn(OH)_6$ Hollow Structures with Multilevel Interiors. *Sci. Rep.* **3**, 1391; DOI:10.1038/srep01391 (2013).